

# Second Harmonic Generation from 3D Metallic Networks

Racheli Ron<sup>1</sup>, Omer Shavit<sup>1</sup>, Hannah Aharon<sup>1</sup>, Marcin Zielinski<sup>2</sup>, Matan Galanty<sup>1</sup>, and Adi Salomon<sup>1\*</sup>

1. Department of Chemistry, Institute of Nanotechnology and Advanced Materials (BINA), Bar-Ilan University, Ramat-Gan 5290002, Israel.

2. Attolight AG, EPFL Innovation Park, Building D, 1015 Lausanne, Switzerland.

## Corresponding author

\*Dr. Adi Salomon. [Email: adi.salomon@biu.ac.il](mailto:adi.salomon@biu.ac.il).

## KEYWORDS

Second harmonic generation, nanoporous metals, disordered robust optical system, hot-spots, plasmonics, cathodoluminescence.

## ABSTRACT

Second-harmonic-generation is forbidden from most bulk metals, because metals are characterized by a net zero electric-field in equilibrium. Yet, fabrication of a three-dimensional macroscale metallic piece comprising sub-wavelength features remains a challenge for many years. Herein, we introduce a nanoporous metallic network whose building-blocks are assembled into an effective nonlinear conductive material, with conversion efficiency of about  $5.5 \times 10^{-11}$ . The high nonlinear response results from the network structure, which permit connectivity between the various active photonic elements. The nanoscale building-blocks are connected to each other

forming a robust network and respond in a collective manner to form very intense hot-spots. Broadband responses of the metallic network are observed both by second-harmonic-generation and cathodoluminescence. The large-scale dimension and generation of randomized hot-spots make this three-dimensional metallic network a promising candidate for applications like photocatalysis, sensing, or in optical imaging as structured illumination microscopy.

## INTRODUCTION

In a disordered network system the building-blocks are randomly connected. This leads to a higher-level architecture, and the system may respond in a collective manner.<sup>1,2</sup> If large enough in size, the network becomes robust so that a local damage does not lead to a system failure.<sup>3,4</sup> Such robust disordered networks are of great importance in photonic devices, because they can respond in a cooperative manner to the applied electromagnetic (EM) field. In nature, corals are an example for such a robust disordered system, where light is diffusively scattered enabling symbiotic algae to capture a large fraction of photons and optimize subaquatic photosynthetic energy production.<sup>5</sup>

Such three-dimensional (3D) structures made of metals are absent in Nature, and their production which comprises nanoscale features remains challenging even with current technology.<sup>6-11</sup> The lack in techniques for preparing sufficiently pure and robust *metallic* networks has slowed down the optical investigation of these interesting disordered structures.<sup>12</sup> Nonetheless, the potential of such metallic networks systems both in photonics and in catalysis has been recognized.<sup>7,11,13-15</sup> Three-dimensional disordered metallic nanostructures display a rich variety of optical phenomena.<sup>2,7,11,16</sup> Their random architecture with a broad nano-size and shape ranges of holes and particles results in EM field enhancement over a wide range of the optical spectrum. Moreover, their surface curvature and texture changes at the submicron scale, and therefore the EM field lines either converge or diverge, leading to refraction-index modulation

at the submicron scale.<sup>4,15</sup> Typically, in such metallic networks there are regions with very high electron density, which thus exhibit strong local fields. These regions lead to excitation of localized plasmonic modes, and are referred as ‘hot-spots’.<sup>17</sup> In addition, the connectivity between the building-blocks, such as nanoparticles, allows these networks to support propagating plasmonic modes.<sup>18</sup> As a result of surface plasmons (SPs) excitation, inherently weak nonlinear optical processes such as Raman scattering<sup>19,20</sup> and second harmonic generation (SHG)<sup>21–24</sup> can be boosted by orders of magnitudes. Indeed, enhanced SHG from disordered metallic islands was already observed at 1981.<sup>25</sup> Nonetheless, thus far reported SH emissions from such disordered systems as well as from 3D metallic system are rather low.<sup>26–39</sup> Two main reasons are put forward to explain this observation; one is low number of hot-spots, which are generally disconnected and therefore, their induced EM field does not overlap. The other one is the phase randomization of the emitted field that results from the incoherent hyper Rayleigh scattering (HRS) rather than the coherent SHG process.<sup>22,40</sup>

Recently, we have developed a technique to fabricate large-scale 3D disordered nanoporous metallic networks (see [Figure 1](#)).<sup>9</sup> The technique is based on physical vapor deposition (PVD) onto an electrostatic silica aerogel substrate (see [Methods](#) section). These networks are made of chain-like ligaments with typical dimensions of about 100 nm, forming a continuous solid framework with multi-size and -shape pores. A key property of these disordered networks is that they combine large numbers of two optically active elements: pores and nanoparticles, that both support plasmonic excitation over a broad optical frequency range. We think that the connectivity between these optical elements enables excitation of collective eigenmodes, which give rise to intense hot-spots.<sup>2</sup>

Herein, we experimentally study SHG responses of a robust disordered 3D metallic network made of silver, illuminated in normal angle (Figure 1a). The SHG responses from such a network are relatively high, with emission of about 200k counts per second (CPS) of blue photons from about  $0.5 \times 0.5 \mu\text{m}^2$  hot-spot area, in any given polarization state of the fundamental field and in several fundamental wavelengths (FWs). The observed high SHG arises from connectivity between individual nanoparticles, which are coupled to each other and thus emit coherently forming larger size hot-spots. Cathodoluminescence (CL) measurements support this observation, showing multiple emission hot-spots over a broad range of wavelengths.

## **RESULTS AND DISCUSSION**

### **Characteristics of the SHG response from the 3D network**

Figures 1b-d display scanning electron microscopy (SEM) images of typical nanoporous silver networks. Three-dimensional entangled ligaments form a continuous percolating solid network. Sizes of the interconnected pores range from 5 nm to 500 nm, and thus permit permeability of both materials and energy. Morphologically, each ligament in the network is a string of metallic nano-size particles, around 100 nm thick, which are firmly connected by means of solid fusion. The variety in sizes and shapes of the optical elements forming the network should lead to a broadband spectral and high nonlinear responses, because both the fundamental and the emitted second harmonic fields are potentially enhanced.

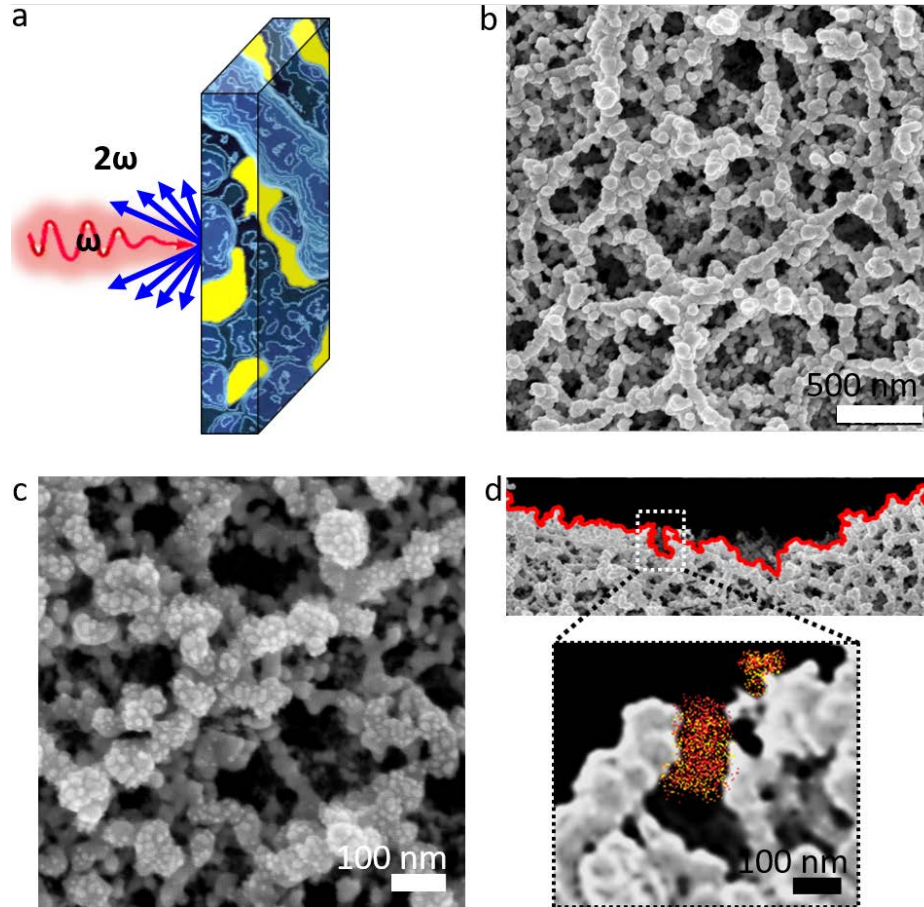


**Figure 1. The 3D metallic network.** (a) Illustration of a 3D disordered metallic network. When light impinges the nanoporous network surface, plasmonic modes can be excited at different frequencies due to broad size and shape ranges of both holes (yellow) and particles (blue). A concomitant EM field enhancement within the 3D silver network both at the fundamental and at the SH frequency is expected. (b-c) SEM images of 3D silver network (top views). The average ligament size lies at about 100 nm, whereas cavities are multi-size (5-500 nm). (c) Networks are covered by <10 nm metallic tips that strongly enhance light confinement at the metallic nanostructures constituting the 3D network. (d) Cross-sectional SEM image of the 3D silver network showing two different types of hot-spots as is illustrated for a nanoparticle and a gap.

In order to study the nonlinear optical response of the network, samples were excited in reflection mode by a tunable Ti:Sapphire laser (690–1080 nm, 100 fs pulse duration, 80 MHz repetition rate) using  $\times 50/0.5\text{NA}$  air objective at normal angle. A schematic illustration of the SHG set-up is shown in supporting information (SI) Section SA. In short, samples were mounted on a piezo stage, and were scanned along both x and y axes. The laser power was set at 1.5 mW at

the laser exit, and SHG intensities along two perpendicular polarization directions were measured by directing the reflected light via a polarizing beam splitter onto two avalanche photodiodes (APDs).

Characteristic SHG emission from a silver network is shown in [Figures 2a-b](#). Clearly, an intense SHG emission is observed from certain confined areas, the so-called ‘hot-spots’. High-resolution SEM images revealed that the network ligaments are covered by <10 nm tip-shaped nanoparticles as is clearly seen in [Figure 1c](#). This thorny texture contributes significantly to enhancing EM field densities at these sharp metallic tips. The hot-spots are spatially localized into sub-micron scale areas, and their apparent size is diffraction-limited by our set-up. Magnitudes of the emitted SHG signal from the silver network, without considering losses along the optical path, are in the order of 20,000 CPS. For comparison, the SHG signal from a continuous silver film exhibits no more than 500 CPS from both APDs under the same fundamental wavelength power settings (1.5 mW, 0.5 NA objective), lying close to the noise level of the APDs, see [SI Section SB](#). That is, these metallic networks generate an enhanced SHG emission, which is at least 45 times stronger comparing to a thin silver film (see detailed information in [SI Section SB](#)).

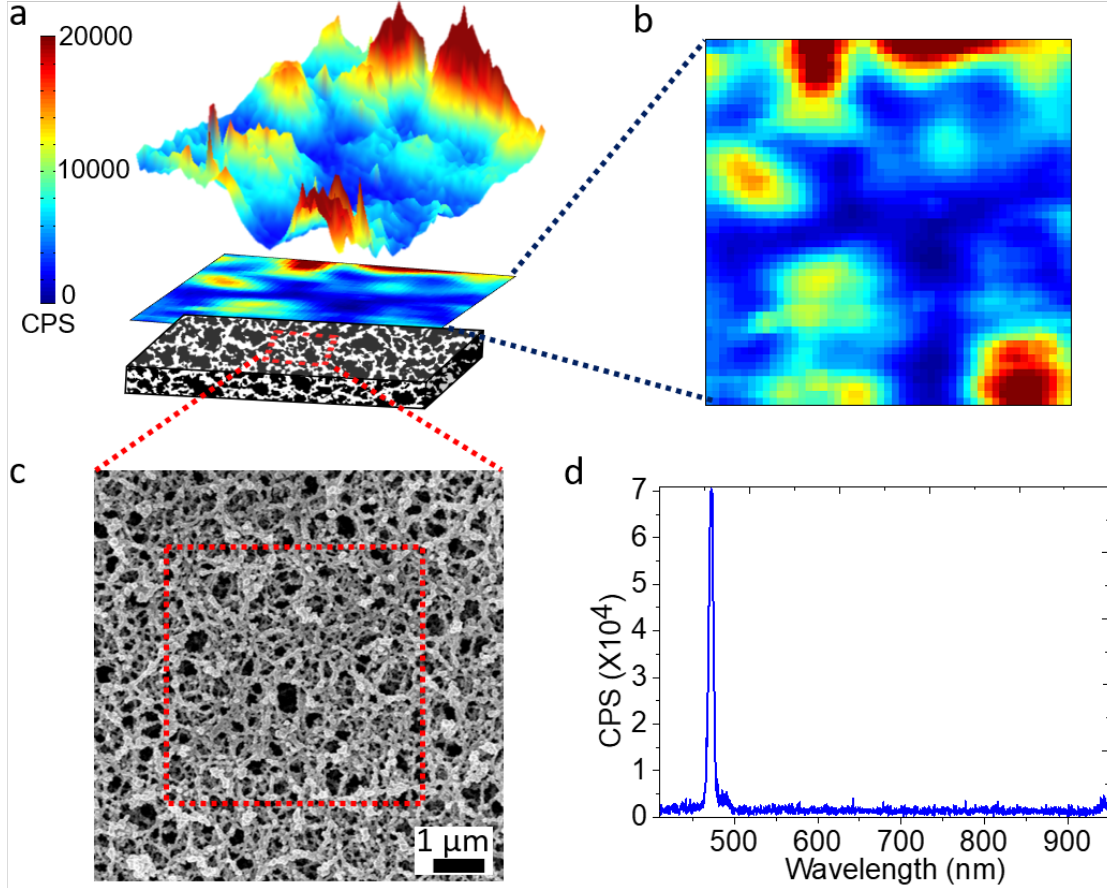


**Figure 2. SHG response of the metallic network.** (a-b) SHG response of the nanoporous silver network over  $5 \times 5 \mu\text{m}^2$  scan area as is indicated in the SEM image in (c). (d) SHG emission spectrum under incident fundamental beam of 940 nm indicating that processes other than SHG are negligible.

Considering the inversion symmetry of the silver lattice, only negligible SHG response is expected due to symmetry breaking at the surface. However, our reported silver networks combine two optically active elements: metallic nanoparticles and nanocavities, the two support localized SP excitations over the whole optical range- both at the fundamental and at SH frequencies. The high density of photonic modes is one of the reasons for such an efficient SHG process. In addition, the connectivity between the optically active building-blocks may enable collective responses throughout the network. As well, we note that in such disordered system a diffused scattering may

be observed leading to high SHG intensity towards the backscattering direction comparing with all other directions (see [SI Section SC](#)).<sup>41,42</sup>

Typical spectral characteristics of the emitted SHG signal are shown in [Figure 2d](#). A sharp SHG peak at 470 nm is observed with minute residual signal of the fundamental field pointing out the reliability of our optical system. No luminescence or other multi-photon processes are observed, indicating that the collected photons resulted solely from SHG. The expected quadratic intensity dependence of SHG is shown in [Figure S2](#). Additionally, the SHG conversion efficiency from the silver networks was evaluated to be  $5.6 \times 10^{-11}$ , taking into account losses along the detection path in our experimental set-up. See [SI Section SD](#) for calculation details. This resulted value is relatively high comparing to reported SHG conversion efficiency in other works.<sup>43-45</sup>

To emphasize the structural uniqueness of these metallic networks, we measured the SH response from a denser silver network, which is mostly lack of percolating pores. A typical SHG emission from a denser silver network is displayed in [Figure 3](#). Of note, localized sub-micrometer scale hot-spots are neither detected from continuous silver films nor from denser silver networks. Clearly, the network porosity and density affect its optical performance. The SHG response from a denser silver network is relatively uniform over the scanned area with minor hot-spots, and introduces a lower average signal which is one order of magnitude smaller compared to the SHG signal from our studied nanoporous network. We postulate that the few observed hot-spots from the denser silver networks are assigned to areas in which the network is relatively less dense or quite rough.

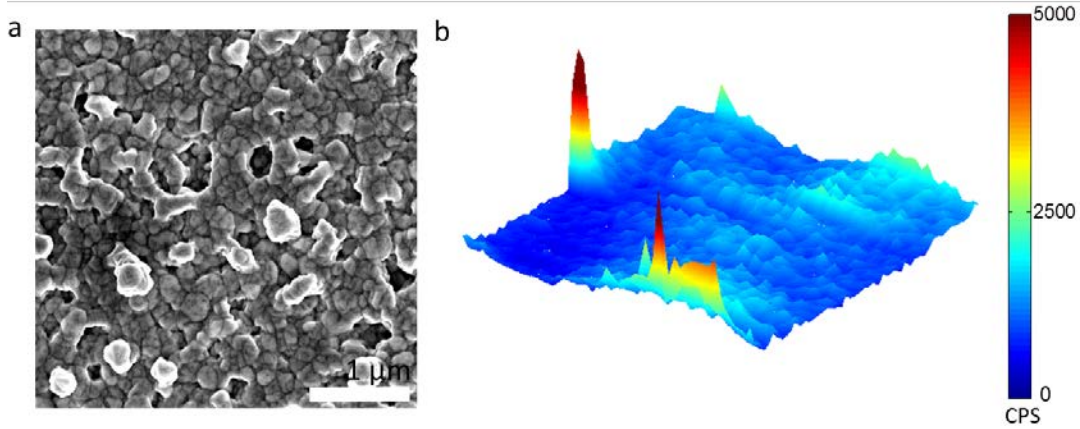


**Figure 3. Effect of the network density on SHG responses.** (a) SEM image of a dense silver network. (b) SHG response of a typical dense silver network ( $5 \times 5 \mu\text{m}^2$ ). The SHG signal is relatively uniform over the scanned area with minor hot-spots and a lower average signal of about 2500 CPS. Measurements were carried out under identical conditions of 940 nm fundamental wavelength and 1.5 mW power. Two-dimensional presentation of the SHG scan is shown in [SI section SE](#).

### Coherent SHG emission

To study the nature of the 3D silver network hot-spots and their nonlinear response we measured the SHG emission at two output orthogonal polarizations over a large scan of  $5 \times 5 \mu\text{m}^2$ . The SHG emissions and the set-up scheme are shown in [Figure 4](#). For simplicity, we present two cases of  $1 \times 1 \mu\text{m}^2$  scans at two *output* polarizations (the full scans are shown in [Figure S6](#)). In the first case, the nonlinear response is dependent on the output polarization ([Figure 4b](#)). That is, while high nonlinear responses are observed for *p output* polarization, the response is suppressed for *s output* polarization. This can be explained by non-coherent nonlinear response, HRS. That is, the optical elements which contribute to the emission are not coupled to each other and behaved individually, and therefore the observed emission is moderate. In this case nonlinear response is correlated with the sum of the optical elements, rather than with the square of them as in the case of SHG. On the other hand, [Figure 4c](#) shows the case in which the nonlinear responses are very similar regardless of the output polarization, with some magnitude variations. This observation

illustrates a typical behavior of our studied networks, as is shown in the full scans (Figure S6). We postulate that the observed hot-spots are composed of coupled optical elements, such as a chain of coupled nanoparticles, and thus behave as a single unit. This is illustrated in Figure 4d.

This result is also demonstrated by the SHG emission line-scans versus position at two orthogonal output polarizations over the 3D silver network (Figures 4g). This behavior is one of the reasons for the observed strong nonlinear response, since it is distinct from the incoherent HRS process, which is barely observed here (see Figure S6 for the full scans). SHG from multiple oscillating dipoles or ensembles of metallic nanoparticles were barely observed before,<sup>44,46,47</sup> due to phase randomization arising from defects and host materials, or because the particles were too distant to permit coupling. Following that, lower nonlinear responses were observed, due to the incoherent HRS process rather than the coherent SHG process.<sup>44</sup> Herein, we suggest that several optical elements are coupled to each other through the network connectivity and form larger and intense hot-spots.

The connectivity between the optical elements is supported by CL measurement of the 3D silver network. Figures 4e-f show CL scans of about  $1.5 \times 1.5 \mu\text{m}^2$  at wavelengths of  $725(\pm 50)$  nm and  $470(\pm 5)$  nm, respectively. Several hot-spots are shown. Few are localized to an area of about  $140 \text{ nm} \times 170 \text{ nm}$ , whereas others are delocalized to a larger area of about  $700 \text{ nm} \times 500 \text{ nm}$ . No correlation between the network morphology and the CL is observed, in agreement with Losquin *et al.*<sup>48</sup>

The network nanostructure is accompanied by giant refraction index fluctuations at the sub-micrometer scale. This refraction index inhomogeneity induces a prominent EM localization, which is mediated by plasmons excitation.<sup>4,15</sup> Concentration of the EM energy at sharp nanometer size tips form thereby hot-spots of peak field intensities. These intense EM peaks function as local

nonlinear sources for SHG. Nevertheless, we believe that the network structure permits connectivity and cooperativity between the metallic sources generating a large hot-spot. That is, the networking has a functional role in the observed enhanced nonlinear response from this nonporous silver structure.

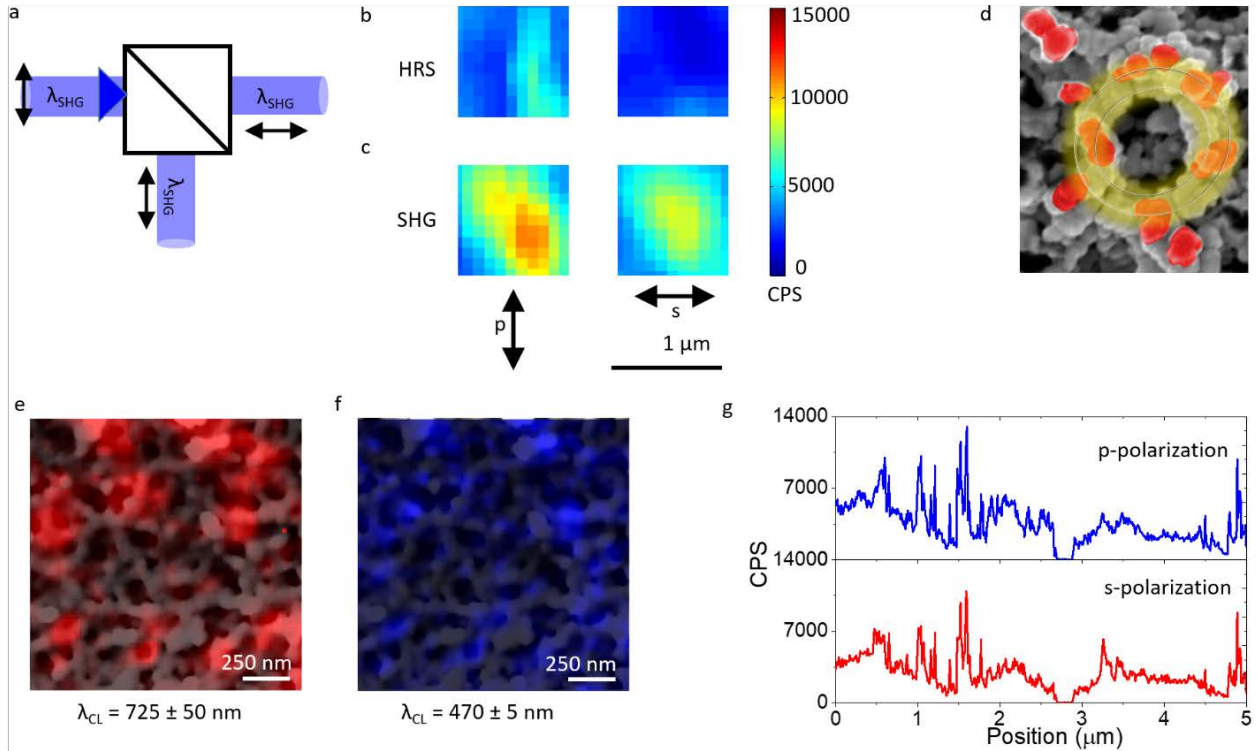


**Figure 4. Coherent SHG from the silver Network.** (a) The SHG signal emitted from the silver networks is directed into a beam-splitter, and is collected in two orthogonal output polarizations. (b-c) Nonlinear responses at orthogonal polarizations from  $1 \times 1 \mu\text{m}^2$  silver network areas. The dissimilarity between the nonlinear responses of the same network area at the two orthogonal polarizations shown in (b) indicates an HRS process, different from the case of SHG process which is shown in (c). (d) Illustration of coupling between the optical active elements in the network due to its inherent structural connectivity. (e-f) CL images showing the emission at (e)  $725(\pm 50) \text{ nm}$  and (f)  $470(\pm 5) \text{ nm}$  from the same silver network, which is shown by the overlapping SEM image of the network. (g) Line-scans over the 3D silver network measuring orthogonally polarized SHG emission versus position. An extended overlap between the plots at both polarizations indicating coherent SHG emission that the 3D nanoporous silver network generates. Experiments were carried out using fundamental wavelength of  $940 \text{ nm}$ .

## Broadband SHG response and spatial localization

The multiple sizes and shapes of metallic nanoparticles and nanoholes result in broadband excitation of plasmonic modes in both visible and near-IR regions of the spectrum.<sup>2,49</sup> Therefore, we expect the silver network to enhance the SHG response at multiple fundamental wavelengths. We shall note that plasmonic modes both at the fundamental and at the SH frequencies can be excited, due to broadband responses.<sup>9,10</sup>

To further investigate the nonlinear response of the silver networks, we performed wavelength-dependent SHG measurements. [Figure 5](#) shows SHG emissions from the *same*  $5 \times 5 \mu\text{m}^2$  silver network upon illumination with three different fundamental wavelengths of 900, 940 and 980 nm. All the other parameters were kept identical, and these wavelengths have been chosen so that the response of our set-up (APDs, filters) is very similar. White contour lines were added at identical locations over the three different SHG scans. This is aimed at facilitating comparison between the wavelength-dependent SHG emissions from the same silver network. An enhanced and localized SHG emissions are detected for all three wavelengths. Yet, the hot-spots appear at different areas of the network are dependent on the fundamental excitation wavelength. For example, the bottom-right hot-spot has its strongest intensity appeared for 940 nm fundamental illumination compared to the other FWs. Whereas, a lower SHG response from this bottom-right network location was observed for 900 nm, and a negligible intensity for 980 nm. Further comparison accompanied by average intensity calculations at different local hot-spots are detailed in [SI Sections SG-H](#). We observed intensity differences of about half an order of magnitude upon the network illumination by the three different FWs. This “on/off” behavior, coming into expression by a fluctuating SHG emission as function of the exciting FW, might be useful for example for structured illumination microscopy (SIM).<sup>50</sup> This is because the hot-spots can be alternatively activated as function of the

FW and polarization. Additionally, since the average size of the building-blocks can be controlled by the physical parameters of the fabrication,<sup>9,10</sup> some tuning of the SHG responses for a specific wavelength might be attained as well.

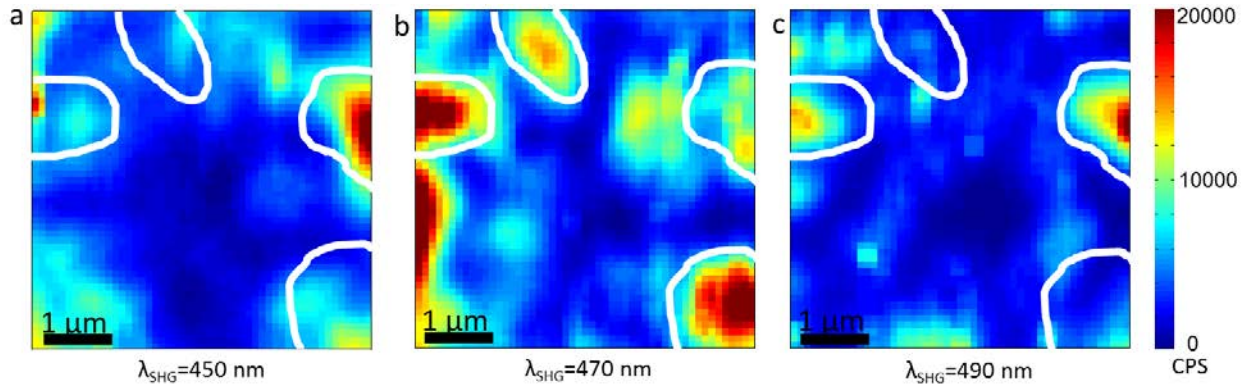


**Figure 5. Wideband SHG response of silver network.** Scanning of  $5 \times 5 \mu\text{m}^2$  SHG responses emanating from 3D silver network under illumination with three different fundamental wavelengths of (a) 900, (b) 940 and (c) 980 nm. Although from the same network area, hot-spots are observed at different locations. The white lines are aimed at facilitating comparison of the nonlinear responses under the different FWs.

The broad optical responses of the nanoporous silver networks are demonstrated by CL measurements as well. A broad optical response of the metallic network is observed, with multiple modes generating from different network locations. CL spectra from three nearby network locations are presented in Figure 6. The resulting color of the large-scale silver metallic network is yellowish (see the inset in Figure 6a), yet CL measurements reveal that different network locations give rise to different optical emission peaks. We attribute the observed spectra to multimode excitations of SPs both from the particles and the pores. The excitation of large number of SP modes increases the density of photonic modes at the interface leading to the observed enhanced nonlinear responses at several fundamental wavelengths.

This broadband linear behavior extends into the IR<sup>2</sup> as evidenced from linear optical measurements (see [Figure S9](#) and ref.<sup>9</sup>), and is meaningful for boosting SHG because it supports mode matching both at the fundamental excitation wavelength and second harmonic wavelength.<sup>43</sup> Hence, the results from both the CL and linear optical analyses point that silver in the form of a nanoporous 3D network is a spectrally dense medium, with confined EM fields locations of energy-modes forming hot-spots. In particular, the disordered network is a multi-resonant architecture and can support intense SHG at several optical wavelengths.

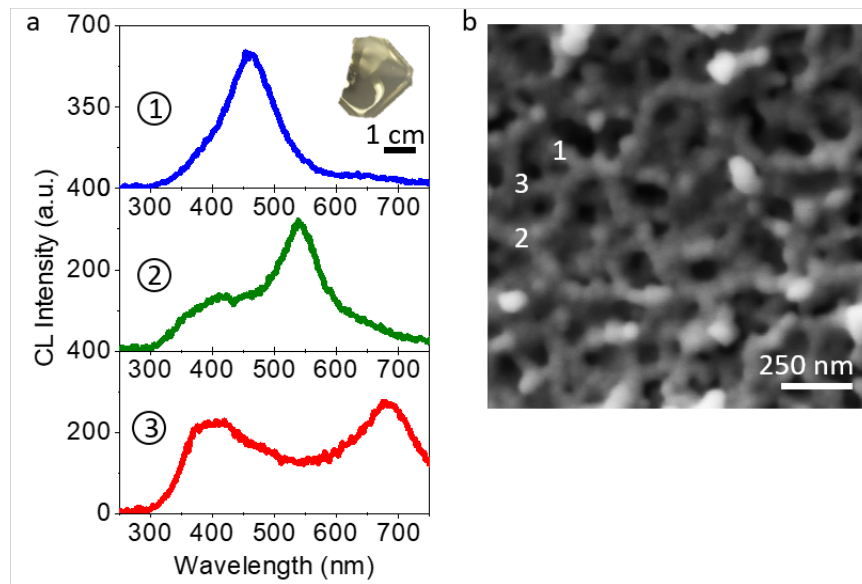


**Figure 6.** Cathodoluminescence emission from 3D silver network. (a) Point CL spectra which were extracted from different spatial locations at the silver network which is shown by the network's SEM image in (b). The CL spectra and network locations are indicated by numbers. The inset optical camera photograph in (a) shows the overall large-scale dimensions and gold-like yellowish color of a typical silver network.

## CONCLUSIONS

Large-scale nanoporous silver networks show a considerable high nonlinear response, both compared to flat silver surface and compared to conventional well defined plasmonic nanostructures.<sup>23,43,44</sup> Furthermore, a confinement of the SHG field into diffraction-limited hot-

spots is observed. The SHG emission is coherent to a large extent, presumably due to the connectivity between the optical active elements. Such network can function as a macroscopic “carpet” of hot-spots, and lead to enhancement of photochemical reactions of molecules located in proximity, or to enhanced detection of molecules. In the context of strong-coupling and energy-transfer processes between plasmonic modes and molecular transition states,<sup>51-53</sup> the metallic network offer a new platform because it can induce long-range interaction between the molecules themselves. Thus, the network plasmonic modes may induce coupling between near and remote molecules and can serve as a ‘pool’ which shape the energy transfer between the molecules themselves.<sup>54,55</sup> Moreover, due to their scalability and optical characteristics these disordered 3D metallic networks are expected to be promising candidates in a wide range of fields including optical sensing, photocatalysis, bio-imaging and photonic devices.

## **MATERIALS AND METHODS**

### **Silver network sample preparation**

Samples of three-dimensional nanoporous silver networks were prepared by sputtering on a silica aerogel substrate, as is detailed elsewhere.<sup>9</sup> In brief, samples preparation comprises two steps: (1) aerogel substrate synthesis, and (2) PVD. Silica aerogels were synthesized by a one-step base-catalyzed sol-gel process followed by CO<sub>2</sub> supercritical drying (K850, Quorum). Metals were sputtered (682, Gatan) from pure targets (99.99%, kurt Lesker).

### **SHG measurements**

A schematic illustration of the SHG set-up is shown in [Figure S1a](#). The SHG set-up includes a tunable Ti:sapphire laser (Mai-Tai HP, Spectra Physics, 690-1080 nm) with 100 fs pulse duration and 80 MHz repetition rate. Samples were mounted on a piezoelectric stage with a closed-loop

feedback (Piezosystem Jena), and were scanned with 100 nm step-size along both x and y axes. The laser power was controlled by a Glan-Taylor polarizer, and was set at 1.5 mW. The incident FW was focused on the sample surface by an inverted microscope using a  $\times 50/0.5\text{NA}$  air objective (Olympus) at normal angle. The nominal spot size is 1.1  $\mu\text{m}$ . Detailed calculation and the specific spot size value as function of wavelength are presented in [SI Section SD](#). The SHG signal was collected in reflection mode through the same objective. A dichroic mirror (Chroma) was used to block the reflected fundamental beam, and appropriate band-pass filters were used to further isolate the SH radiation. The reflected light was directed via a polarizing beam splitter onto two APDs (Perkin-Elmer) to measure the SHG intensity along two perpendicular polarization directions (channels 1 and 2). The nominal noise level of the APDs is 200 CPS. To measure the spectrum, the emitted SHG signal was focused onto the entrance slit of a spectrograph (303i, Shamrock) equipped with an electron multiplied charge-coupled device camera (Andor Newton).

### **CL measurements**

CL measurements were performed by an Attolight Rosa 4634 CL microscope (Attolight AG, Switzerland), which tightly integrates a high numerical aperture 0.72 NA achromatic reflective lens within the objective lens of a field-emission-gun scanning electron microscope (FEG-SEM). The focal plane of the light lens matches the FEG-SEM optimum working distance. CL was spectrally resolved using a Czerny-Turner spectrometer (320 mm focal length, 150 grooves per mm grating) and measured with a UV–visible CCD camera. Acceleration voltage of 10 kV, and electron beam emission current of 20 nA were applied.

### **ACKNOWLEDGEMENTS**

We thank prof. M. Oheim for carefully reading the manuscript.

## FUNDING

This work was supported by the Israeli Prime Minister office via the INREP project, and by the Energy and Water Resources Ministry of Israel grant number 216-11-016.

## REFERENCES

- (1) Shalaev, V. M.; Poliakov, E. Y.; Markel, V. A. Small-Particle Composites. II. Nonlinear Optical Properties. *Phys. Rev. B* **1996**, *53*, 2437–2449.
- (2) Shalaev, V. M.; Safonov, V. P.; Poliakov, E. Y.; Markel, V. A.; Sarychev A. K. Fractal-Surface-Enhanced Optical Nonlinearities. In: *Nanostructured Materials*; Shalaev V. M., Moskovits, M., Eds.; ACS Symposium Series: San Francisco, 1997; pp 88–107.
- (3) Albert, R.; Jeong, H.; Barabási, A.-L. Error and Attack Tolerance of Complex Networks. *Nature* **2000**, *406*, 378–382.
- (4) Galinski, H.; Fratolocchi, A.; Döbeli, M.; Capasso, F. Light Manipulation in Metallic Nanowire Networks with Functional Connectivity. *Adv. Opt. Mater.* **2017**, *5*, 1600580.
- (5) Marcelino, L. A.; Westneat, M. W.; Stoyneva, V.; Henss, J.; Rogers, J. D.; Radosevich, A.; Turzhitsky, V.; Siple, M.; Fang, A.; Swain, T. D.; et al. Modulation of Light-Enhancement to Symbiotic Algae by Light-Scattering in Corals and Evolutionary Trends in Bleaching. *PLoS One* **2013**, *8*, , e61492.
- (6) Kränzlin, N.; Niederberger, M. Controlled Fabrication of Porous Metals from the Nanometer to the Macroscopic Scale. *Mater. Horizons* **2015**, *2*, 359–377.
- (7) Biener, J.; Nyce, G. W.; Hodge, A. M.; Biener, M. M.; Hamza, A. V.; Maier, S. A. Nanoporous Plasmonic Metamaterials. *Adv. Mater.* **2008**, *20*, 1211–1217.
- (8) Herrmann, A.-K.; Formanek, P.; Borchardt, L.; Klose, M.; Giebeler, L.; Eckert, J.; Kaskel,

- S.; Gaponik, N.; Eychmüller, A. Multimetallic Aerogels by Template-Free Self-Assembly of Au, Ag, Pt, and Pd Nanoparticles. *Chem. Mater.* **2014**, *26*, 1074–1083.
- (9) Ron, R.; Gachet, D.; Rechav, K.; Salomon, A. Direct Fabrication of 3D Metallic Networks and Their Performance. *Adv. Mater.* **2017**, *29*, 1604018.
- (10) Racheli Ron, Emir Haleva, A. S. Nanoporous Metallic Networks: Fabrication, Optical Properties and Applications. *Adv. Mater.* **2018**, 1706755.
- (11) Ding, Y.; Zhang, Z. Nanoporous Metals. In: *Springer Handbook of Nanomaterials*; Vajtai, R., Ed.; Springer: Berlin, 2013; pp 779–818.
- (12) Lee, W.-K.; Yu, S.; Engel, C. J.; Reese, T.; Rhee, D.; Chen, W.; Odom, T. W. Concurrent Design of Quasi-Random Photonic Nanostructures. *Proc. Natl. Acad. Sci. U. S. A.* **2017**, *114*, 8734–8739.
- (13) Ding, Y.; Chen, M. Nanoporous Metals for Catalytic and Optical Applications. *MRS Bull.* **2009**, *34*, 569–576.
- (14) Zhang, J.; Li, C. M. Nanoporous Metals: Fabrication Strategies and Advanced Electrochemical Applications in Catalysis, Sensing and Energy Systems. *Chem. Soc. Rev.* **2012**, *41*, 7016.
- (15) Galinski, H.; Favraud, G.; Dong, H.; Gongora, J. S. T.; Favaro, G.; Döbeli, M.; Spolenak, R.; Fratolocchi, A.; Capasso, F. Scalable, Ultra-Resistant Structural Colors Based on Network Metamaterials. *Light Sci. Appl.* **2016**, *6*, e16233.
- (16) Wiersma, D. S. Disordered Photonics. *Nat. Photonics* **2013**, *7*, 188–196.
- (17) Novotny, L.; Hecht, B. Surface plasmons. In *Principles of nano-optics*; Cambridge University Press: Cambridge, 2006; pp 378-418.
- (18) Yu, F.; Ahl, S.; Caminade, A. M.; Majoral, J. P.; Knoll, W.; Erlebacher, J. Simultaneous Excitation of Propagating and Localized Surface Plasmon Resonance in Nanoporous Gold

- Membranes. *Anal. Chem.* **2006**, *78*, 7346–7350.
- (19) Zhang, Q.; Large, N.; Nordlander, P.; Wang, H. Porous Au Nanoparticles with Tunable Plasmon Resonances and Intense Field Enhancements for Single-Particle SERS. *J. Phys. Chem. Lett.* **2014**, *5*, 370–374.
- (20) Solís, D. M.; Taboada, J. M.; Obelleiro, F.; Liz-Marzán, L. M.; García De Abajo, F. J. Toward Ultimate Nanoplasmonics Modeling. *ACS Nano* **2014**, *8*, 7559–7570.
- (21) Boardman, A. D.; Zayats, A. V. Nonlinear Plasmonics. *Handb. Surf. Sci.* **2014**, *4*, 329–347.
- (22) Butet, J.; Brevet, P.-F.; Martin, O. J. F. Optical Second Harmonic Generation in Plasmonic Nanostructures: From Fundamental Principles to Advanced Applications. *ACS Nano* **2015**, *9*, 10545–10562.
- (23) Salomon, A.; Zielinski, M.; Kolkowski, R.; Zyss, J.; Prior, Y. Size and Shape Resonances in Second Harmonic Generation from Silver Nanocavities. *J. Phys. Chem. C* **2013**, *117*, 22377–22382.
- (24) van Nieuwstadt, J. A. H.; Sandtke, M.; Harmsen, R. H.; Segerink, F. B.; Prangma, J. C.; Enoch, S.; Kuipers, L. Strong Modification of the Nonlinear Optical Response of Metallic Subwavelength Hole Arrays. *Phys. Rev. Lett.* **2006**, *97*, 146102.
- (25) Wokaun, A.; Bergman, J. G.; Heritage, J. P.; Glass, A. M.; Liao, P. F.; Olson, D. H. Surface Second-Harmonic Generation from Metal Island Films and Microlithographic Structures. *Phys. Rev. B* **1981**, *24*, 849–856.
- (26) Argyrakis, P.; Kopelman, R.; Arbor, A. Observation of Weak Localization of Light in a Random Medium. **1986**, *44*, 1047–1048.
- (27) Smolyaninov, I.; Zayats, A.; Davis, C. Near-Field Second Harmonic Generation from a Rough Metal Surface. *Phys. Rev. B* **1997**, *56*, 9290–9293.

- (28) Metzger, B.; Gui, L.; Fuchs, J.; Floess, D.; Hentschel, M.; Giessen, H. Strong Enhancement of Second Harmonic Emission by Plasmonic Resonances at the Second Harmonic Wavelength. *Nano Lett.* **2015**, *15*, 3917–3922.
- (29) Beermann, J.; Bozhevolnyi, S. I. Microscopy of Localized Second-Harmonic Enhancement in Random Metal Nanostructures. *Phys. Rev. B* **2004**, *69*, 155429.
- (30) Bozhevolnyi, S. I.; Beermann, J.; Coello, V. Direct Observation of Localized Second-Harmonic Enhancement in Random Metal Nanostructures. *Phys. Rev. Lett.* **2003**, *90*, 197403.
- (31) Ginzburg, P.; Krasavin, A.; Sonnefraud, Y.; Murphy, A.; Pollard, R. J.; Maier, S. A.; Zayats, A. V. Nonlinearly Coupled Localized Plasmon Resonances: Resonant Second-Harmonic Generation. *Phys. Rev. B* **2012**, *86*, 085422.
- (32) Stockman, M. I.; Bergman, D. J.; Anceau, C.; Brasselet, S.; Zyss, J. Enhanced Second-Harmonic Generation by Metal Surfaces with Nanoscale Roughness: Nanoscale Dephasing, Depolarization, and Correlations. *Phys. Rev. Lett.* **2004**, *92*, 057402.
- (33) Breit, M.; Podolskiy, V. A.; Grésillon, S.; von Plessen, G.; Feldmann, J.; Rivoal, J. C.; Gadenne, P.; Sarychev, A. K.; Shalaev, V. M. Experimental Observation of Percolation-Enhanced Nonlinear Light Scattering from Semicontinuous Metal Films. *Phys. Rev. B* **2001**, *64*, 125106.
- (34) Anceau, C.; Brasselet, S.; Zyss, J.; Gadenne, P. Local Second-Harmonic Generation Enhancement on Gold Nanostructures Probed by Two-Photon Microscopy. *Opt. Lett.* **2003**, *28*, 713-715.
- (35) Krachmalnicoff, V.; Castanié, E.; De Wilde, Y.; Carminati, R. Fluctuations of the Local Density of States Probe Localized Surface Plasmons on Disordered Metal Films. *Phys. Rev.*

- Lett.* **2010**, *105*, 183901.
- (36) Pollard, R. J.; Murphy, A.; Hendren, W. R.; Evans, P. R.; Atkinson, R.; Wurtz, G. A.; Zayats, A. V.; Podolskiy, V. A. Optical Nonlocalities and Additional Waves in Epsilon-near-Zero Metamaterials. *Phys. Rev. Lett.* **2009**, *102*, 127405.
- (37) Mascheck, M.; Schmidt, S.; Silies, M.; Yatsui, T.; Kitamura, K.; Ohtsu, M.; Leipold, D.; Runge, E.; Lienau, C. Observing the Localization of Light in Space and Time by Ultrafast Second-Harmonic Microscopy. *Nat. Photonics* **2012**, *6*, 293–298.
- (38) Zayats, a V; Smolyaninov, I. I.; Davis, C. C. Observation of Localized Plasmonic Excitations in Thin Metal Films with Near-Field Second-Harmonic Microscopy. *Opt. Commun.* **1999**, *169*, 93–96.
- (39) Simon, H. J.; Mitchell, D. E.; Watson, J. G. Optical Second-Harmonic Generation with Surface Plasmons in Silver Films. *Phys. Rev. Lett.* **1974**, *33*, 1531–1534.
- (40) Johnson, R. C.; Li, J.; Hupp, J. T.; Schatz, G. C. Hyper-Rayleigh Scattering Studies of Silver, Copper, and Platinum Nanoparticle Suspensions. *Chem. Phys. Let.* **2002**, *356*, 534–540.
- (41) Gaponenko, S. V. Light in non-periodic structures. In *Introduction to nanophotonics*. Cambridge University Press: Cambridge, 2010; pp 246-294.
- (42) Wolf, P. E.; Maret, G. Weak Localization and Coherent Backscattering of Photons in Disordered Media. *Phys. Rev. Lett.* **1985**, *55*, 2696–2699.
- (43) Celebrano, M.; Wu, X.; Baselli, M.; Großmann, S.; Biagioni, P.; Locatelli, A.; De Angelis, C.; Cerullo, G.; Osellame, R.; Hecht, B.; et al. Mode Matching in Multiresonant Plasmonic Nanoantennas for Enhanced Second Harmonic Generation. *Nat. Nanotechnol.* **2015**, *10*, 412–417.

- (44) Salomon, A.; Prior, Y.; Fedoruk, M.; Feldmann, J.; Kolkowski, R.; Zyss, J. Plasmonic Coupling between Metallic Nanocavities. *J. Opt.* **2014**, *16*, 114012.
- (45) Galanty, M.; Shavit, O.; Weissman, A.; Aharon, H.; Gachet, D.; Segal, E.; Salomon, A. Second Harmonic Generation Hotspot on a Centrosymmetric Smooth Silver Surface. *Light Sci. Appl.* **2018**, *7*, 49.
- (46) Smythe, E. J.; Cubukcu, E.; Capasso, F. Optical Properties of Surface Plasmon Resonances of Coupled Metallic Nanorods. *Opt. Express* **2007**, *15*, 7439–7447.
- (47) Slablab, A.; Le Xuan, L.; Zielinski, M.; de Wilde, Y.; Jacques, V.; Chauvat, D.; Roch, J.-F. Second-Harmonic Generation from Coupled Plasmon Modes in a Single Dimer of Gold Nanospheres. *Opt. Express* **2012**, *20*, 220.
- (48) Losquin, A.; Camelio, S.; Rossouw, D.; Besbes, M.; Pailloux, F.; Babonneau, D.; Botton, G. A.; Greffet, J.-J.; Stéphan, O.; Kociak, M. Experimental Evidence of Nanometer-Scale Confinement of Plasmonic Eigenmodes Responsible for Hot Spots in Random Metallic Films. *Phys. Rev. B* **2013**, *88*, 115427.
- (49) Markel, V. A.; Shalaev, V. M.; Stechel, E. B.; Kim, W.; Armstrong, R. L. Small-Particle Composites. I. Linear Optical Properties. *Phys. Rev. B* **1996**, *53*, 2425–2436.
- (50) Gustafsson, M. G. L. Surpassing the Lateral Resolution Limit by a Factor of Two Using Structured Illumination Microscopy. *J. Microsc.* **2000**, *198*, 82–87.
- (51) Efremushkin, L.; Bhunia, S. K.; Jelinek, R.; Salomon, A. Carbon Dots Plasmonics Coupling Enables Energy Transfer and Provides Unique Chemical Signatures. *J. Phys. Chem. Lett.* **2017**, *8*, 6080–6085.
- (52) Sukharev, M.; Seideman, T.; Gordon, R. J.; Salomon, A.; Prior, Y. Ultrafast Energy Transfer between Molecular Assemblies and Surface Plasmons in the Strong Coupling

- Regime. *ACS Nano* **2014**, *8*, 807–817.
- (53) Salomon, A.; Gordon, R. J.; Prior, Y.; Seideman, T.; Sukharev, M. Strong Coupling between Molecular Excited States and Surface Plasmon Modes of a Slit Array in a Thin Metal Film. *Phys. Rev. Lett.* **2012**, *109*, 073002.
- (54) Pustovit, V. N.; Shahbazyan, T. V. Resonance Energy Transfer near Metal Nanostructures Mediated by Surface Plasmons. *Phys. Rev. B* **2011**, *83*, 085427.
- (55) Andrew, P.; Barnes, W. L. Energy Transfer across a Metal Film Mediated by Surface Plasmon Polaritons. *Science* **2004**, *306*, 1002–1005.



# Supporting Information

## Second Harmonic Generation from 3D Metallic Networks

Racheli Ron<sup>1</sup>, Omer Shavit<sup>1</sup>, Hannah Aharon<sup>1</sup>, Marcin Zielinski<sup>2</sup>, Matan Galanty<sup>1</sup>, and Adi Salomon<sup>1\*</sup>

1. Department of Chemistry, Institute of Nanotechnology and Advanced Materials (BINA), Bar-Ilan University, Ramat-Gan 5290002, Israel.

2. Attolight AG, EPFL Innovation Park, Building D, 1015 Lausanne, Switzerland.

### SA. SHG experimental set-up

#### Second harmonic generation measurements

A schematic illustration of the SHG set-up is shown in [Figure S1a](#). The SHG set-up includes a tunable Ti:sapphire laser (Mai-Tai HP, Spectra Physics, 690-1080 nm) with 100 fs pulse duration and 80 MHz repetition rate. Samples were mounted on a piezoelectric stage with a closed-loop feedback (Piezosystem Jena), and were scanned with 100 nm step-size along both x and y axes. The laser power was controlled by a Glan-Taylor polarizer, and was set at 1.5 mW. The incident FW was focused on the sample surface by an inverted microscope using a  $\times 50/0.5\text{NA}$  air objective (Olympus) at normal angle. The nominal spot size is 1.1  $\mu\text{m}$ . Detailed calculation and the specific spot size value as function of wavelength are presented in [SI Section SD](#). The SHG signal was collected in reflection mode through the same objective. A dichroic mirror (Chroma) was used to block the reflected fundamental beam, and appropriate band-pass filters were used to further isolate the SH radiation. The reflected light was directed via a polarizing beam splitter onto two APDs (Perkin-Elmer) to measure the SHG intensity along two perpendicular polarization directions (channels 1 and 2). The nominal noise level of the APDs is 200 CPS. To measure the spectrum, the emitted SHG signal was focused onto the entrance slit of a spectrograph (303i, Shamrock) equipped with an electron multiplied charge-coupled device camera (Andor Newton).

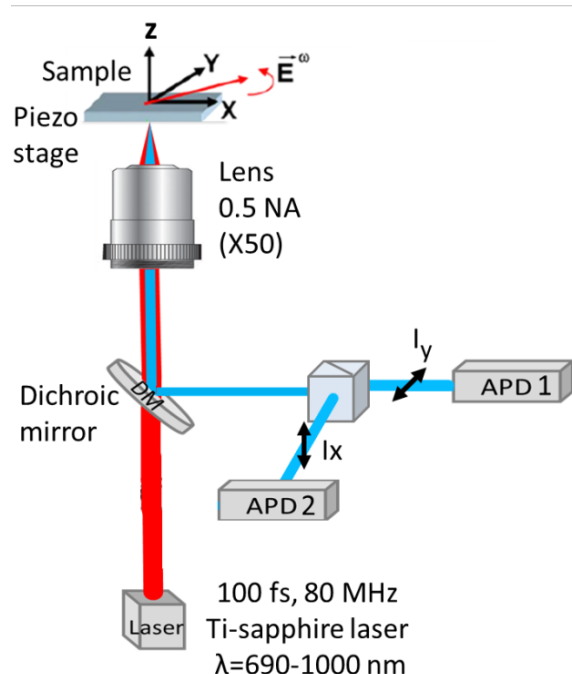


**Figure S1.** Illustration of our SHG experimental set-up. The sample is mounted on a piezoelectric stage and is scanned along both  $x$  and  $y$  axes. A focused beam from a Ti-sapphire laser of 100 fs pulse duration and 80 MHz repetition rate is directed to the sample using 0.5 NA and  $\times 50$  magnification objective, and the SH signal is collected in a reflection mode by the same objective. The reflected light is directed to a polarizing beam splitter. The two perpendicular polarization components of the SHG signal are detected by two calibrated APDs, channel 1 and channel 2.

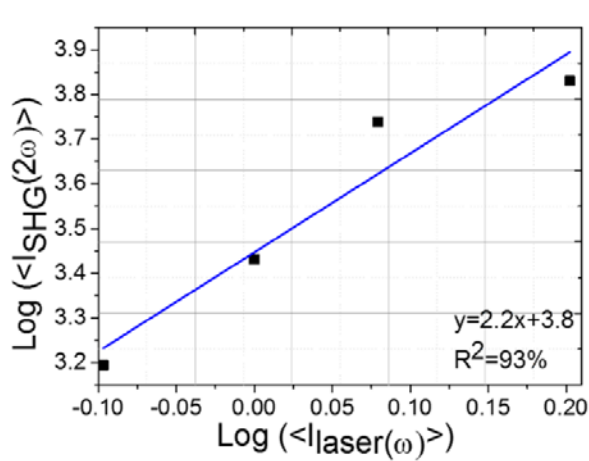


**Figure S2.** Quadratic relation between input fundamental laser and output SHG intensities as expected for such nonlinear process. Slope of about 2 between the input laser power and output SHG signal was achieved with 93% linear fitting.

## SB. Comparison between SHG responses emanating from a silver film versus a silver network

SHG signals at orthogonal polarizations from a silver film and a silver network are presented in Figure S2.

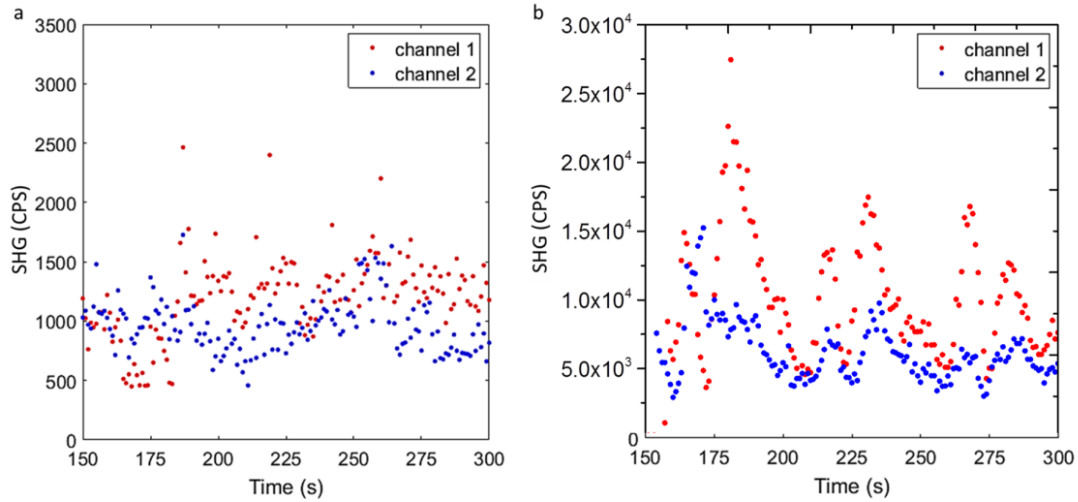


**Figure S3.** SHG response from (a) thin silver film and (b) a silver network. SHG signal was collected by two APDs (channels 1 and 2) placed at orthogonal polarizations under fundamental wavelength illumination of 940 nm. Double power was applied for the silver film measurement, comparing to silver networks measurements, in order to be able to detect a clear signal. Note the different scales in (a) and (b), which are aimed at facilitating observation.

Based on the fact that  $P^2(\omega) \propto P(2\omega)$ , an enhancement of  $\times 45$  is obtained comparing SHG response of a silver network versus that of a thin silver film, see [Table S1](#).

**Table S1.** SHG responses from a silver film and a silver network, *without taking losses into consideration*.

	Input power (mW)	Measured SHG signal* (CPS)	Expected SHG signal for 10 mW input power* (CPS)
<b>Silver film</b>	10	2,000	2,000
<b>Silver network</b>	1.5	20,000	89,000

\*Sum of two orthogonal polarization channels.

## SC. Directional reflection from disordered metallic nanostructures

Pronounced multiple scattering occurs in a disordered media. Reflection through these nanoporous metallic networks does not necessarily decay exponentially with thickness.<sup>1,2</sup> With respect to scattering, both the mean pore size and the mean grain size are expected to play important roles, because they determine how photons migrate through the network. The pore size will determine the scattering mean free path whereas the particle size will impact the scattering anisotropy, that is, the distribution of scattering angles following each scattering event. If the pores are large, the free path between two scattering events might be large enough to permit faint scattering, leading to closed loop photon trajectories and *enhanced reflection*. In this case, the output intensity is relatively high, because the probability of photons to exit the material with a trajectory similar to the original one, after multiple scattering events, is relatively high.

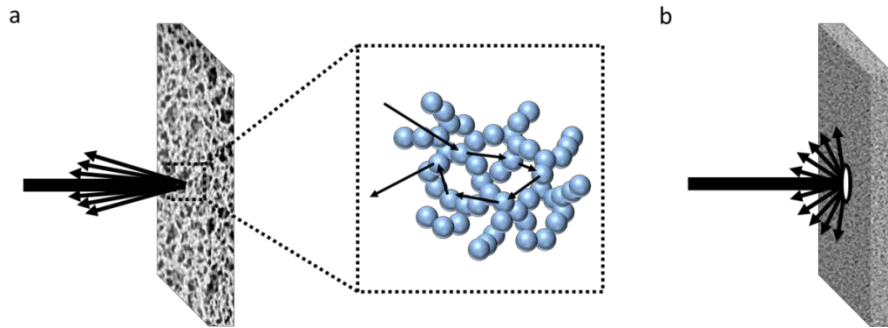


**Figure S4. Light propagation in disordered structures.** When pore sizes are large enough closed loop photon migration might arise. (a) Light scattering through metallic networks can be directional towards the backscattering direction (b) versus widely scattered.

## SD. Losses consideration in our set-up

### Laser beam intensity and power

Input SHG experimental parameters and laser power calculations are presented in [Table S2](#).

**Table S2. Input experimental parameters.**

Parameter	Fundamental wavelength (nm)	Laser repetition rate (MHz)	Laser pulse length (fs)	Objective numerical aperture	Laser power (average) (mW)	Laser peak power (W)
Symbol/ Equation	$\lambda$	$\nu$	$\tau$	NA	$\langle P_{FW} \rangle$	$\hat{P}_{FW} = \frac{\langle P_{FW} \rangle}{\tau}$
Value	940	80	100	0.5	1.5	187.5

Average intensity of the irradiating laser beam is  $\langle I_{FW} \rangle = \frac{\langle P_{FW} \rangle}{A_{obj(\omega)}} = 3.63 \times 10^8 \text{ (W/m}^2\text{)}$ .

$A_{obj}$  denotes the spot area of the objective lens. The exciting spot diameter is  $\delta(\omega) = \frac{1.22\lambda}{NA} = 2.29 \text{ (}\mu\text{m)}$  for  $\lambda_{FW}=940 \text{ nm}$ . The exciting spot area at the focus of the laser is  $A_{obj} = \pi(r_\omega)^2 = 4.13 \times 10^{-12} \text{ (m}^2\text{)}$ ,  $r_\omega$  is the radius of the illuminated area under FW illumination. Peak intensity of the irradiated laser is  $\hat{I}_{FW} = \frac{\hat{P}_{FW}}{A_{obj(\omega)}} = 4.54 \times 10^{13} \text{ (W/m}^2\text{)}$ , with regards to the laser peak power of 625 W and  $A_{obj}$  at 940 nm.

We evaluated our system transmittance to be able to compare our SHG enhancement with others. To evaluate efficiency of SHG emission from the 3D silver networks, we considered the losses along the optical path length in our experimental set-up. First, the total transmittance of our experimental set-up at 470 nm is evaluated; only 70% of the incoming light is transmitted through the optical components including lenses, four filters, dichroic mirror, and polarizing beam splitter. The efficiency of the APD is 60% at 470 nm. About 80% of the light is coupled to the fiber. Consequently, total transmittance efficiency of our system at 470 nm is  $\sim 10\%$ .

Considering the actual total transmittance of our experimental system, the average SHG emission from the silver networks is higher than **200 kCPS** at  $0.5 \times 0.5 \mu\text{m}^2$  hot-spot area (see as well [Section SG](#) here). Output SHG power calculations and values are detailed in [Table S3](#).

Therefore, we arrive at a peak nonlinear coefficient of  $\gamma_{\text{SHG}} = 3.01 \times 10^{-13} \text{ (W}^{-1}\text{)}$ , and conversion efficiency of  $\eta_{\text{SHG}} = 5.64 \times 10^{-11}$  from the silver networks (Table S4).

**Table S3. Output SHG power calculations considering losses\*.**

Parameter	SHG emitted photons (CPS)	SHG photon energy (J)	SHG Power (W)	SHG Peak power (W)
<b>Symbol/Equation</b>	$\frac{N}{\Delta t}$	$E_{\text{ph,SHG}} = \frac{hc}{\lambda_{\text{SHG}}}$	$\langle P_{\text{SHG}} \rangle = \frac{N}{\Delta t} \cdot E_{\text{ph,SHG}}$	$\hat{P}_{\text{SHG}} = \frac{\langle P_{\text{SHG}} \rangle}{\tau v}$
<b>Network</b>	200,000	$4.23 \times 10^{-19}$	$8.46 \times 10^{-14}$	$1.06 \times 10^{-8}$

\* For 470 nm, at hot-spot.

$E_{\text{ph,SHG}}$  denotes energy of the emitted SHG photon at  $\lambda_{\text{SHG}} = 470 \text{ nm}$ ,  $h = 6.63 \times 10^{-34} \text{ J}\cdot\text{s}$  is Planck constant, and  $c = 3 \times 10^8 \text{ m/s}$  is the speed of light in vacuum.

**Table S4. SHG efficiency calculations considering losses.**

Parameter	Conversion efficiency	Peak Nonlinear Coefficient (W <sup>-1</sup> )
<b>Equation</b>	$\eta_{\text{SHG}} = \frac{\langle P_{\text{SHG}} \rangle}{\langle P_{\text{FW}} \rangle}$	$\gamma_{\text{SHG}} = \frac{\hat{P}_{\text{SHG}}}{(\hat{P}_{\text{FW}})^2}$
<b>Value</b>	$5.64 \times 10^{-11}$	$3.01 \times 10^{-13}$

<sup>1</sup>For 470 nm. Signal at a hot-spot.

## SE. Effect of network density on SHG response

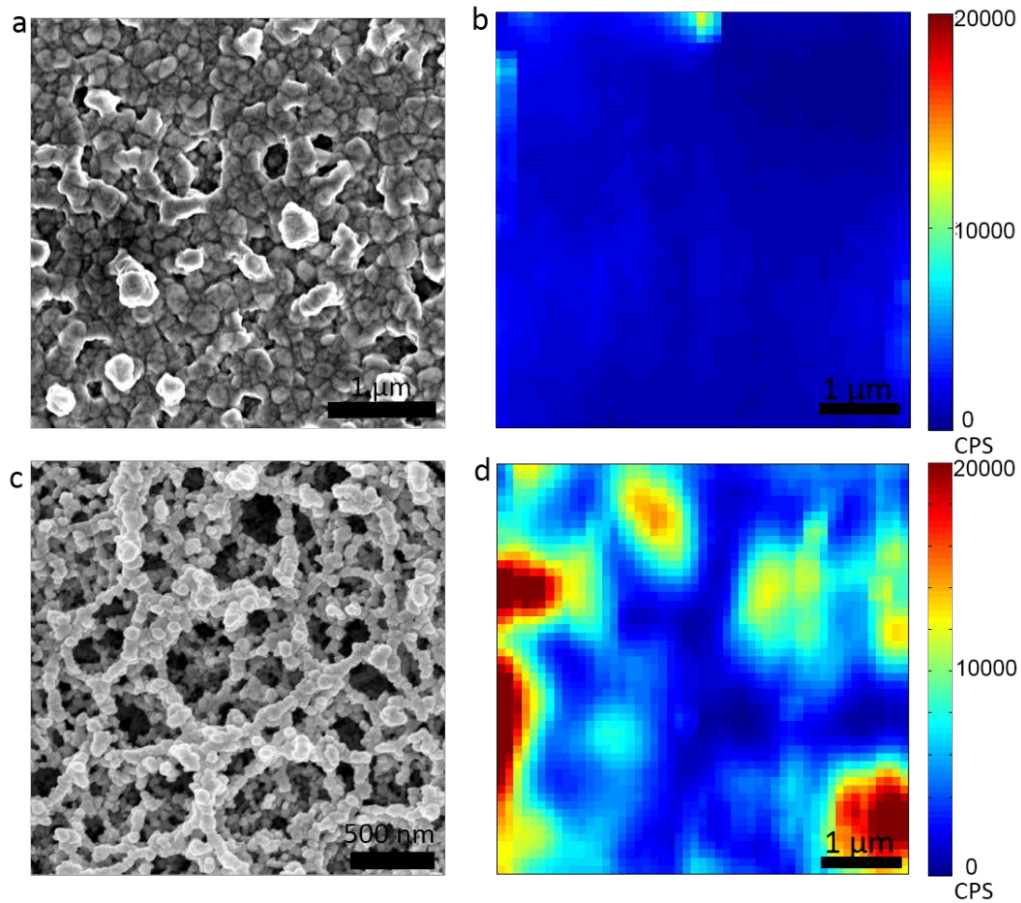


**Figure S5.** SHG response from a dense silver network. (a) SEM image and (b) SHG scan of a dense silver network ( $5 \times 5 \mu\text{m}^2$  area). To facilitate comparison, our typical 3D silver network is shown in (c) with its typical SHG response in (d). SHG signal from the dense network is relatively uniform over the scanned area with minor hot-spots.

**SF. SHG responses of the same area in a given network as function of the output polarization**

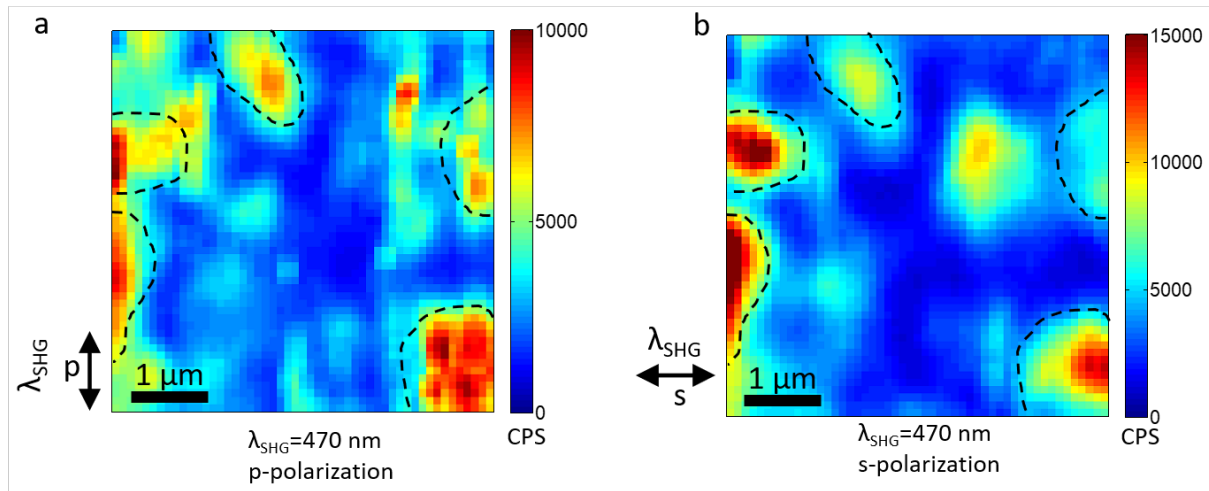


**Figure S6. Coherent SHG from the silver Network.** (a-b) SHG responses at orthogonal polarizations from the same silver network area ( $5 \times 5 \mu\text{m}^2$ ). The similarity between the SHG responses at the two output polarizations reveals a coherent emission in such disordered system. The black guidelines on the scans and the different scale-bars aimed at facilitating observation.

### SG. SHG responses of the same area in a given network excited by three different fundamental wavelengths

Scanning SHG response of a given  $5 \times 5 \mu\text{m}^2$  area of a silver network shows that SHG hot-spots are observed at different locations as function of the fundamental wavelength illumination. In order to quantitatively evaluate the dependence of SHG response on exciting wavelength, average SHG intensities for each fundamental wavelength were calculated (Figure S7a). Considering the whole  $5 \times 5 \mu\text{m}^2$  scanned network area (noted by black squares in Figures S7b-d), the highest average SHG emission was generated under 940 nm illumination.

More interesting, we calculated average SHG emissions from two different  $1 \times 1 \mu\text{m}^2$  network areas; one is of rather *low* emission noted by central white squares in Figures S7b-d, and the second area is of *fluctuating* SHG emission as function of the illumination wavelength, noted by bottom-right yellow squares.

The central spots generate a relatively lower SHG emission under the three different fundamental wavelengths comparing to the two other mentioned hot-spots. However, their average SHG intensity is on the order of 2000-4000 CPS, which is higher emission level compared to previous works measured SHG from silver nanoparticles or nanoholes<sup>3,4</sup>.

The bottom-right yellow squares introduce an “*on/off*” *behavior* of the SHG responses as function of fundamental wavelengths. That is, the average SHG intensity is ~16,000 CPS for 940 nm fundamental wavelength, which is about  $\times 2$  and  $\times 4$  times higher than for 900 and 980 nm fundamental wavelengths, respectively. These results demonstrate the broadband nonlinear response of a single 3D nanoporous silver network.

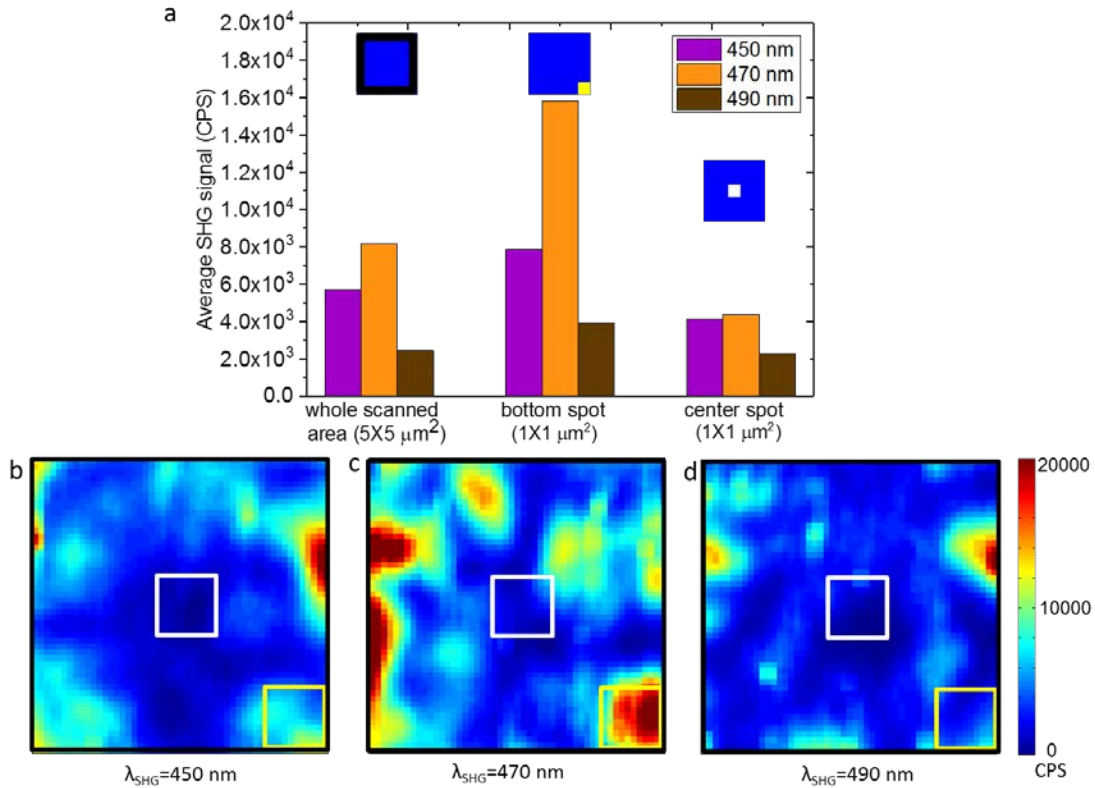


**Figure S7.** Average SHG emission from the same silver network under three different fundamental wavelengths. (a) The histogram presents mean SHG intensity of three different network *areas*, and for each examined fundamental *wavelength* of (b) 900 nm (c) 940 nm, and (d) 980 nm. Locations are indicated by colored squares: *white* 1 × 1 μm<sup>2</sup> center spot, *yellow* 1 × 1 μm<sup>2</sup> bottom-right spot, and *black* square for the whole 5 × 5 μm<sup>2</sup> scanned network area.

## SH. Calculation of average SHG signal at different hot-spot locations

Here we compare the average SHG signal at different intense hot-spot areas. The average SHG signal at three different  $0.5 \times 0.5 \mu\text{m}^2$  hot-spot locations under 940 nm fundamental wavelength illumination and 1.5 mW power was calculated (see Figure S8).

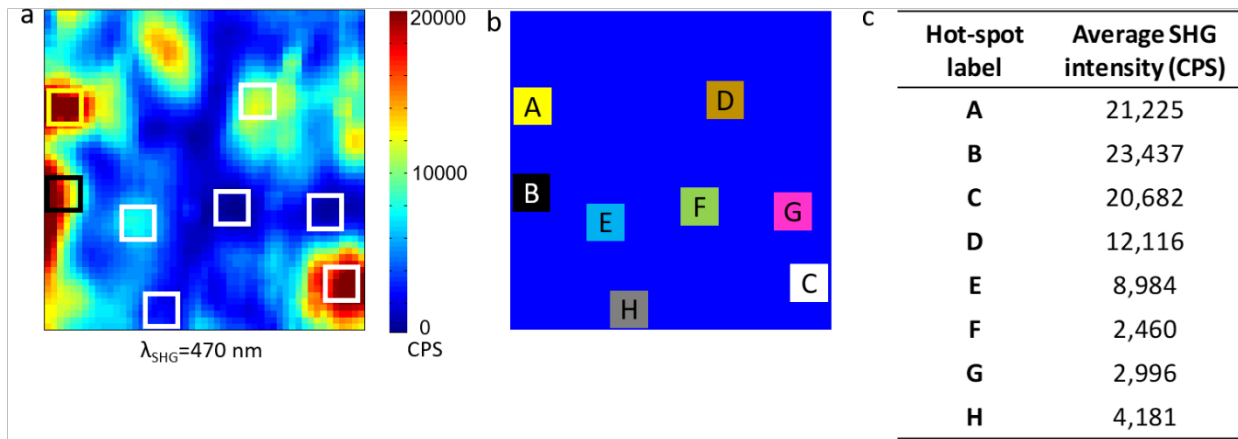


**Figure S8.** Average SHG emission from three different intense hot-spots. Hot-spot size is  $0.5 \times 0.5 \mu\text{m}^2$ . The hot-spots are indicated on the SHG scan of the silver network in (a), and their locations are illustrated in (b). (c) Tabulated values of mean SHG intensity at each spot. Sum SHG signal from two channels was considered.

## SI. Linear optical measurements

Experimentally, optical imaging was carried out using an inverted light microscope (IX83, Olympus) in transmission mode employing a  $\times 100/0.90\text{NA}$  air objective (Olympus). Transmission spectra were acquired using a Bio-100 spectrophotometer (CARY). Spectra were normalized against the transmission through a pristine aerogel substrate on a glass-slide under identical optical conditions.

A broad optical response of the metallic network is observed, with transmission gradually increasing towards the IR region. We compared the linear optical properties of the network to that of a silver thin film (40 nm thickness). As opposed to the silver network, transmission of the silver film was higher at the short visible wavelengths and much lower at the longer visible wavelengths, as expected.

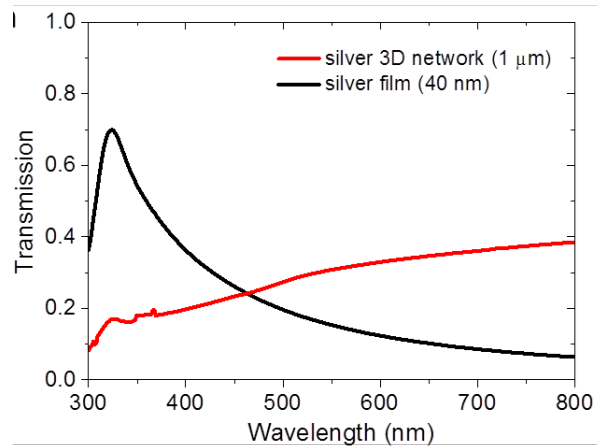


**Figure S9. Linear optical response of 3D silver network and film.** Linear transmission spectra of 1  $\mu\text{m}$  thick silver network and of 40 nm silver film for comparison.

## Supporting References

- (1) Gaponenko, S. V. Light in non-periodic structures. In *Introduction to nanophotonics*. Cambridge University Press: Cambridge, 2010; pp 246-294.
- (2) Jacques, S. L. Optical properties of biological tissues: a review. *Phys. Med. Biol.* **2013**, *58*, R37–R61.
- (3) Salomon, A.; Zielinski, M.; Kolkowski, R.; Zyss, J.; Prior, Y. Size and shape resonances in second harmonic generation from silver nanocavities. *J. Phys. Chem. C* **2013**, *117*, 22377–22382.
- (4) Salomon, A.; Prior, Y.; Fedoruk, M.; Feldmann, J.; Kolkowski, R.; Zyss, J. Plasmonic coupling between metallic nanocavities. *J. Opt.* **2014**, *16*, 114012.